

# BRANCHGRPO: STABLE AND EFFICIENT GRPO WITH STRUCTURED BRANCHING IN DIFFUSION MODELS

Yuming Li<sup>1\*</sup> Yikai Wang<sup>2\*</sup> Yuying Zhu<sup>3</sup>  
 Zhongyu Zhao<sup>1</sup> Ming Lu<sup>1</sup> Qi She<sup>3</sup> Shanghang Zhang<sup>1</sup>  
<sup>1</sup>Peking University <sup>2</sup>Beijing Normal University <sup>3</sup>ByteDance

## ABSTRACT

Recent progress in aligning image and video generative models with Group Relative Policy Optimization (GRPO) has improved human preference alignment, yet existing approaches still suffer from high computational cost due to sequential rollouts and large numbers of SDE sampling steps, as well as training instability caused by sparse rewards. In this paper, we present BranchGRPO, a method that restructures the rollout process into a branching tree, where shared prefixes amortize computation and pruning removes low-value paths and redundant depths. BranchGRPO introduces three contributions: (1) a branch sampling scheme that reduces rollout cost by reusing common segments; (2) a tree-based advantage estimator that converts sparse terminal rewards into dense, step-level signals; and (3) pruning strategies that accelerate convergence while preserving exploration. On HPDv2.1 image alignment, BranchGRPO improves alignment scores by up to **16%** over strong baselines, while reducing per-iteration training time by nearly **55%**. On WanX-1.3B video generation, it further achieves higher Video-Align scores with sharper and temporally consistent frames compared to DanceGRPO. Codes and models are available at BranchGRPO.

## 1 INTRODUCTION

Diffusion and flow-matching models have advanced image and video generation with high fidelity, diversity, and controllability (Ho et al., 2020; Lipman et al., 2022; Liu et al., 2022). However, large-scale pretraining alone cannot ensure alignment with human intent, as outputs often miss aesthetic, semantic, or temporal expectations. Reinforcement learning from human feedback (RLHF) addresses this gap by directly adapting models toward human-preferred outcomes (Ouyang et al., 2022).

Within RLHF, Group Relative Policy Optimization (GRPO) has shown strong stability and scalability across text-to-image and text-to-video tasks (Liu et al., 2025a; Xue et al., 2025). However, when applied to diffusion and flow-matching models, current GRPO variants still face two fundamental bottlenecks: (1) **Inefficiency**. Standard GRPO adopts a sequential rollout design, where each trajectory must be independently sampled under both the old and new policies. This incurs  $O(N \cdot T)$  complexity with denoising steps  $T$  and group size  $N$ , leading to significant computational redundancy and limiting scalability in large-scale image and video generation tasks. (2) **Sparse rewards**. Most methods compute only a single reward from the final denoised image or video and propagate it uniformly across all denoising steps. This trajectory-level supervision neglects informative signals contained in intermediate states, resulting in unstable optimization, inaccurate credit assignment, and high-variance gradients. This raises a central challenge: *how can we accurately attribute sparse outcome rewards to the specific denoising steps that truly contribute to high-quality generations?*

To overcome these limitations, we propose **BranchGRPO**, a tree-structured policy optimization framework for diffusion and flow models. BranchGRPO replaces inefficient independent sequential rollouts with a branching structure, where scheduled *split steps* in the denoising process allow each trajectory to stochastically expand into multiple sub-trajectories while reusing shared prefixes. This design amortizes computation across common segments and aligns naturally with the stepwise nature of denoising, substantially improving sampling efficiency while reducing computational cost.

\*Equal contribution.

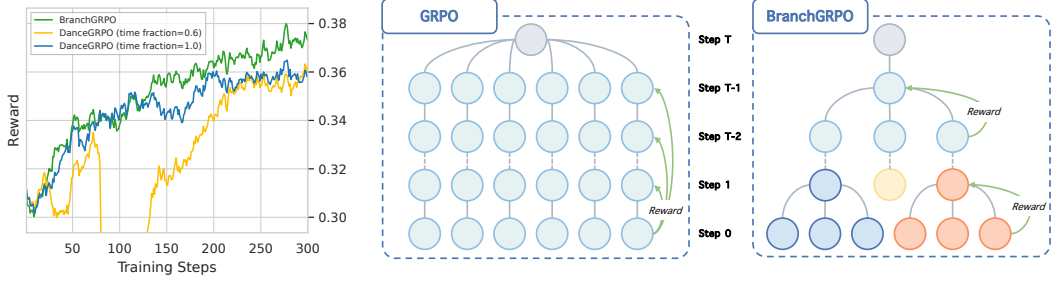


Figure 1: **Comparison of BranchGRPO and DanceGRPO.** *Left:* Reward curves during training. BranchGRPO converges substantially faster, achieving up to  $2.2\times$  **speedup** over DanceGRPO (time fraction = 1.0) and  $1.5\times$  **speedup** over DanceGRPO (time fraction = 0.6), while ultimately surpassing both baselines. The time fraction = 1.0 variant further exhibits pronounced instability. *Right:* Illustration of rollout structures. GRPO relies on sequential rollouts with only final rewards, whereas BranchGRPO performs branching at intermediate steps and propagates dense rewards backward, enabling more efficient and stable optimization.

Crucially, the tree structure enables a novel *reward fusion and depth-wise advantage estimation* mechanism. Instead of assigning a single terminal reward to every denoising step, BranchGRPO aggregates rewards from leaf nodes predicted by the reward model and propagates them backward through depth-wise normalization. This produces layer-wise advantages that allow for finer-grained credit assignment and more stable policy optimization. In addition, BranchGRPO integrates *width- and depth-level pruning strategies* that remove low-value or redundant branches. These pruning mechanisms accelerate training, reduce computational overhead, and enhance effective exploration by reallocating resources to promising regions of the trajectory space.

Our contributions are threefold:

- We introduce BranchGRPO, a tree-structured rollout framework that replaces independent sequential sampling with branching trajectories. By inserting split points during denoising, trajectories expand into multiple sub-trajectories while sharing early prefixes, which reduces redundancy and improves exploration efficiency.
- We propose a new reward fusion and depth-wise advantage estimation method that converts sparse terminal rewards into dense, step-level signals, yielding more stable optimization.
- We design complementary width- and depth-pruning strategies that lower backpropagation cost and further improve alignment.
- We validate the effectiveness of BranchGRPO on both text-to-image and image-to-video alignment tasks, demonstrating its general applicability across modalities.

## 2 RELATED WORK

Diffusion models (Ho et al., 2020; Rombach et al., 2022) and flow matching models (Lipman et al., 2022; Liu et al., 2022) have become dominant paradigms for visual generation due to their strong theoretical foundations and ability to generate high-quality content efficiently. While pretraining establishes the generative prior, aligning outputs with nuanced human preferences requires reinforcement learning from human feedback (RLHF). In natural language processing, RLHF has proven highly successful for aligning large language models (LLMs) (Ouyang et al., 2022; Christiano et al., 2017), where methods such as PPO and GRPO enable stable preference-driven post-training. These successes have inspired adaptation of RLHF to vision.

In the visual domain, RLHF for diffusion has been developed along two main directions. Reward-model-based approaches such as ImageReward (Xu et al., 2023) backpropagate learned rewards through the denoising process. Direct Preference Optimization (DPO) (Rafailov et al., 2023) has also been extended to diffusion, leading to Diffusion-DPO (Wallace et al., 2024) and Videodpo (Liu et al., 2025c), which achieve competitive alignment without explicit reward modeling. Policy-gradient formulations such as DDPO (Black et al., 2023) and DPOK (Fan et al., 2023) further explore

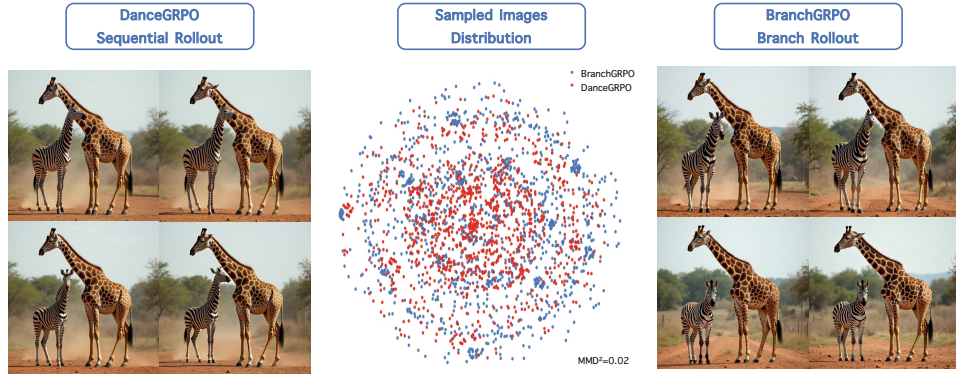


Figure 2: Comparison of sequential and branch rollouts. **Left/Right:** example generations from DanceGRPO and BranchGRPO, respectively. **Middle:** distribution of sampled images projected into 2D feature space, where red and blue dots correspond to DanceGRPO and BranchGRPO. The distributions largely overlap ( $\text{MMD}^2=0.019$ , computed using Maximum Mean Discrepancy (Gretton et al., 2012)), showing that branch rollouts preserve generation diversity.

online optimization but often face stability challenges. Meanwhile, standardized reward models including HPS-v2.1 (Wu et al., 2023), VideoAlign (Liu et al., 2025b) enable systematic comparison of alignment algorithms on image and video tasks.

More recently, Group Relative Policy Optimization (GRPO) (Shao et al., 2024) has been introduced as a scalable alternative to PPO for preference optimization. DanceGRPO (Xue et al., 2025) pioneers the application of GRPO to visual generation, unifying diffusion and flow models via SDE reformulation and demonstrating stable optimization across text-to-image, text-to-video, and image-to-video tasks. Flow-GRPO (Liu et al., 2025a) extends GRPO to flow matching models by introducing ODE-to-SDE conversion and denoising reduction for improved efficiency. MixGRPO (Li et al., 2025a) further enhances efficiency with a mixed ODE–SDE sliding-window scheme, though it still faces trade-offs between overhead and performance. Our work continues this line by introducing BranchGRPO, which leverages branching rollouts, depth-wise reward fusion, and structured pruning to improve both stability and efficiency; while related to TreePO in LLMs (Li et al., 2025b), our method adapts tree-structured rollouts specifically to diffusion dynamics.

### 3 METHOD

#### 3.1 DOES BRANCH ROLLOUT HARM DIVERSITY?

One natural concern with branch rollout is that sharing early prefixes may reduce sample diversity, as multiple leaves originate from the same root trajectory. To examine this, we compare the distribution of images generated by sequential rollouts (DanceGRPO) and our proposed branch rollouts. Figure 2 shows sampled images along with a 2D visualization of feature embeddings. We compute the squared Maximum Mean Discrepancy ( $\text{MMD}^2$ ) between the two distributions as a quantitative measure of diversity. The result,  $\text{MMD}^2=0.019$ , indicates negligible divergence between branch and sequential rollouts. This demonstrates that branch sampling does not compromise diversity, while enabling more efficient exploration and denser reward assignment.

#### 3.2 BRANCH ROLLOUT ALGORITHM

**Preliminaries.** Given a prompt, BranchGRPO reformulates denoising into a tree-structured process. We align terminology with tree search: (i) depth  $T$  denotes the number of denoising steps; (ii) width  $w$  is the number of completed trajectories (leaves); (iii) branching steps  $B$  indicate split timesteps; (iv) branch correlation  $s$  controls the correlation among child noises; (v) branching factor  $K$  is the number of children per split.

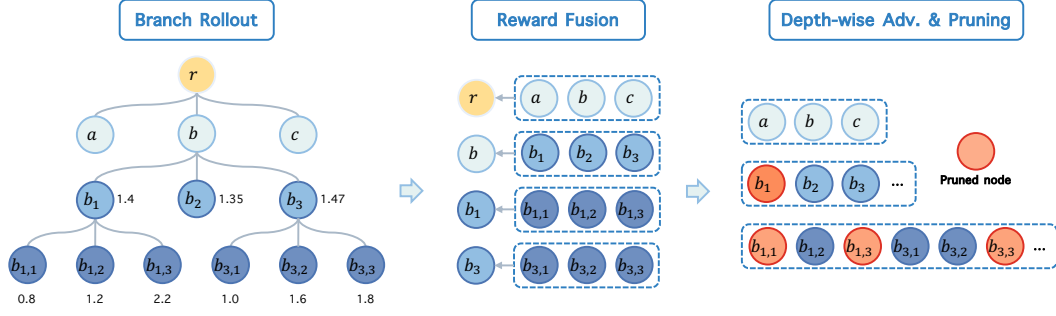


Figure 3: **Left:** branching rollouts generate diverse leaves. **Middle:** leaf rewards are fused upward by path-probability weighting. **Right:** depth-wise normalization and pruning yield dense advantages and reduce cost.

**Branch sampling.** Unlike prior GRPO variants such as DanceGRPO and FlowGRPO that rely on *sequential rollouts*, where each trajectory is sampled independently from start to finish, BranchGRPO reorganizes the process into a tree-structured rollout (Figure 1). For each prompt, we initialize a root node with a same initial noise  $z_0 \sim \mathcal{N}(0, I)$  and then denoise step by step along the reverse SDE. At designated split steps  $\mathcal{B}$ , the current state expands into  $K$  children, producing multiple sub-trajectories that share early prefixes but diverge afterward. The branching is achieved by injecting stochastic perturbations into the SDE transition, with a hyperparameter  $s$  controlling the correlation strength among child noises. This mechanism balances exploration diversity and stability while keeping the marginal distribution unchanged. The rollout continues until reaching the maximum depth  $T$ , at which point all leaves are collected for reward evaluation. Formally, the baseline reverse SDE is

$$dz_t = \left( f(z_t, t) - \frac{1}{2}g^2(t)\nabla \log p_t(z_t) \right) dt + g(t) dw_t, \quad (1)$$

while our branching modification at split step  $i \in \mathcal{B}$  produces

$$z_{i+1}^{(b)} = \mu_\theta(z_i, t_i) + s_i \sqrt{h_i} \xi_b, \quad \xi_b = \frac{\xi_0 + s \delta \xi_b}{\sqrt{1 + s^2}}, \quad b = 1, \dots, K, \quad (2)$$

where  $\xi_0, \delta \xi_b \sim \mathcal{N}(0, I)$  and  $s \geq 0$  adjusts inter-branch correlation. When  $s = 0$ , all branches collapse to a single path, while as  $s \rightarrow \infty$ , the branches become independent. Intuitively, smaller  $s$  yields highly correlated children (stable but limited exploration), whereas larger  $s$  produces more independent trajectories (diverse but noisier).

### 3.3 REWARD FUSION AND DEPTH-WISE ADVANTAGE ESTIMATION

The branch rollout constructs a full trajectory tree in which all leaf nodes share common ancestral prefixes. This shared structure makes it natural to represent the rewards of intermediate nodes through their descendant leaves, analogous to how genetic traits of ancestors can be inferred from their offspring.

In contrast, existing GRPO variants update every denoising step using only the final reward, which ignores informative intermediate states and leads to unstable credit assignment with high variance (see Fig. 3). BranchGRPO leverages its tree structure to overcome this limitation: leaf rewards are propagated upward to internal nodes, normalized layer by layer, and transformed into dense step-wise advantages—without introducing any additional models or computational overhead. Our optimization objective remains a clipped GRPO loss defined on tree edges:

$$J(\theta) = \mathbb{E} \left[ \frac{1}{|\mathcal{E}|} \sum_{e \in \mathcal{E}} \min(\rho_e(\theta) A(e), \text{clip}(\rho_e(\theta), 1 - \epsilon, 1 + \epsilon) A(e)) \right], \quad (3)$$

where  $\mathcal{E}$  denotes tree edges and  $\rho_e(\theta)$  is the importance ratio.

**Reward fusion.** Directly averaging leaf rewards to estimate internal node values can be dominated by rare but noisy trajectories, leading to unstable gradients. To mitigate this, we fuse descendant rewards using path-probability weighting: let  $r_\ell$  be the reward of a leaf  $\ell$ . For an internal node  $n$  with children  $\mathcal{L}(n)$ , we fuse its rewards by

$$\bar{r}(n) = \sum_{\ell \in \mathcal{L}(n)} w_\ell^{(n)} r_\ell, \quad w_\ell^{(n)} = \frac{\exp(\beta s_\ell)}{\sum_{j \in \mathcal{L}(n)} \exp(\beta s_j)}, \quad (4)$$

where  $s_\ell$  is the path log-probability under the behavior policy and  $\beta$  controls the strength of weighting. When  $\beta = 0$ , this reduces to simple averaging; larger  $\beta$  emphasizes high-likelihood paths and reduces the influence of noisy, low-probability leaves, in all our experiments we set  $\beta = 1.0$ .

We consider two alternatives for aggregating leaf rewards. Uniform averaging treats all leaves equally is robust to log-prob calibration errors and encourages exploration by preserving contributions from low-probability leaves. However, it deviates from the expected return under the behavior policy and can introduce high variance when the number of branches is large.

In contrast, path-weighted scheme aligns node-level credit assignment with the behavior distribution, typically reducing variance and yielding more stable updates. Yet, it relies on log-prob calibration and may overly concentrate weight on high-likelihood paths in deep trees. We empirically compare both variants (Sec. 4.4), showing that path weighting improves stability in practice, while uniform averaging provides stronger exploratory diversity.

**Depth-wise normalization.** The tree depth corresponds to denoising steps, and nodes at the same depth share the same noise level. This makes rewards across nodes within a depth directly comparable, while rewards across different depths may differ drastically in scale due to varying noise states. To ensure fair comparison, we normalize aggregated rewards separately within each depth  $d$ :

$$A_d(n) = \frac{\bar{r}(n) - \mu_d}{\sigma_d + \epsilon}, \quad \mu_d = \text{mean}_{n \in \mathcal{N}_d} \bar{r}(n), \quad \sigma_d = \text{std}_{n \in \mathcal{N}_d} \bar{r}(n), \quad (5)$$

where  $\mathcal{N}_d$  denotes the set of nodes at depth  $d$ . Each edge advantage  $A(e)$  is then inherited from its child node and optionally clipped to  $[-A_{\max}, A_{\max}]$ . This per-step standardization aligns gradient magnitudes with the denoising process and prevents deeper nodes from being dominated by shallow ones.

Compared to GRPO’s prompt-level normalization, which uniformly broadcasts a single terminal reward, our branch-based scheme yields *process-dense credit signals* that respect the denoising trajectory. By normalizing rewards at the step level, BranchGRPO produces more stable gradients and more accurate credit assignment to the intermediate denoising steps that truly matter.

### 3.4 PRUNING STRATEGIES

While branch rollouts improve efficiency and provide dense process rewards, an excessive number of branches may induce exponential growth in trajectory count, leading to prohibitive backpropagation cost. Recent work (Li et al., 2025a) has revealed that standard GRPO training contains substantial redundancy and pruning potential. Motivated by this, we introduce two complementary pruning strategies in the context of BranchGRPO: **width pruning**, which reduces the number of leaves used for gradient updates, and **depth pruning**, which skips unnecessary denoising layers.

Importantly, pruning is applied only after reward fusion and depth-wise normalization, and affects backpropagation but not forward rollouts or reward evaluation. This design ensures that all trajectories contribute to reward signals, while gradients are computed only for the selected subset of nodes.

**Width Pruning.** After computing rewards and advantages for all leaves  $\mathcal{L}$ , we optionally select a subset of them for gradient updates. We study two simple modes. The first is *Parent-Top1*, which retains the higher-reward child of each parent in the last branching step. This strategy halves gradient cost while ensuring coverage of all parents, yielding stable but slightly less diverse updates. The second is *Extreme selection*, which preserves both the globally best and worst  $b$  leaves by reward score. By explicitly maintaining strong positive and negative signals, this mode injects more exploratory feedback but introduces higher variance.

---

**Algorithm 1** BranchGRPO Training Process

---

**Require:** dataset  $\mathcal{C}$ ; policy  $\pi_\theta$ ; behavior policy  $\pi_{\theta_{\text{old}}}$ ; reward models  $\{R_k\}$ ; denoising steps  $T$ ; branching steps  $\mathcal{B}$ ; branching factor  $K$ ; branch correlation  $s$

```
1: for iteration  $m = 1$  to  $M$  do
2:    $\pi_{\theta_{\text{old}}} \leftarrow \pi_\theta$ 
3:   Sample batch  $\mathcal{C}_b \subset \mathcal{C}$ 
4:   for prompt  $c \in \mathcal{C}_b$  do
5:     Sample root noise  $z_0 \sim \mathcal{N}(0, I)$ 
6:     Build rollout tree  $\mathcal{T}$  with  $\pi_{\theta_{\text{old}}}$ :
7:     for  $t = T$  to  $0$  do
8:       if  $t \in \mathcal{B}$  then
9:         Branch into  $K$  children with correlation  $s$ 
10:      else
11:        Single-step denoising
12:      end if
13:    end for
14:    Evaluate rewards for leaves  $\mathcal{L}(\mathcal{T})$ 
15:    Reward fusion: aggregate leaf rewards upward (path-prob. weights)
16:    Depth-wise normalization: standardize per depth, assign edge advantages
17:    Pruning (optional): select nodes for backprop only
18:    Compute clipped GRPO loss  $J(\theta)$ 
19:  end for
20:  Update policy: gradient ascent on  $J(\theta)$ 
21: end for
```

---

**Depth Pruning.** Notably, recent work MixGRPO (Li et al., 2025a) achieves strong performance by hybrid ODE–SDE, effectively acting as a form of depth pruning. This motivates our explicit exploration of depth pruning within BranchGRPO.

Specifically, we maintain a set of pruned depths  $\mathcal{D}$  and ignore gradients from nodes at these layers while still performing full forward rollouts for reward evaluation. To avoid permanently excluding certain steps, we employ a *sliding window*: the pruned depths shift gradually toward deeper layers as training progresses, until reaching a predefined maximum depth. Formally, pruning is enabled in all of training steps, and every fixed interval the pruning window slides one step deeper, until reaching a pre-defined stop depth.

This dynamic scheme improves efficiency while still accounting for the contributions of gradients from different depths, thus balancing computational savings with policy effectiveness.

## 4 EXPERIMENTS

### 4.1 EXPERIMENT SETUP

We evaluate BranchGRPO on HPDv2.1 (Wu et al., 2023) (103k training and 400 balanced test prompts). The backbone is FLUX.1-Dev, with rollouts augmented by branching and process-dense rewards; we also study a pruned variant (BranchGRPO-Pruning). Baselines include DanceGRPO and MixGRPO under identical settings. We report efficiency (NFE, iteration time, GPU-hours) and quality (HPS-v2.1, PickScore (Kirstain et al., 2023), ImageReward (Xu et al., 2023)).

### 4.2 IMPLEMENTATION DETAILS

We set the tree depth to  $d = 20$  and the branch factor to  $b = 2$ , yielding 16 leaves per rollout before pruning. The branching steps  $\mathcal{B}$  use three presets: Dense (0, 3, 6, 9) as the default, Mixed (0, 5, 15, 20), and Sparse (0, 10, 13, 19). The branch correlation sweeps  $s \in \{0, 1, 2, 4, 8\}$ . Training runs for 300 optimizer steps with gradient accumulation  $g = 12$  and per-GPU batch size = 2, on  $16 \times$  NVIDIA H20z GPUs. Optimization uses AdamW (learning rate  $1 \times 10^{-5}$ , weight decay





Figure 4: Qualitative comparison of generations from Flux, DanceGRPO, and our BranchGRPO.

Method	$\text{NFE}_{\pi_{\theta_{\text{old}}}}$	$\text{NFE}_{\pi_{\theta}}$	Iteration Time (s)↓	HPS-v2.1↑	Pick Score↑	Image Reward↑
FLUX	-	-	-	0.313	0.227	1.112
DanceGRPO(tf=1.0)	20	20	698	0.360	0.229	1.189
DanceGRPO(tf=0.6)	20	12	469	0.353	0.228	1.219
MixGRPO (20,5)	20	5	<b>289</b>	0.359	0.228	1.211
BranchGRPO	13.68	13.68	493	0.363	0.229	1.233
BranchGRPO-WidPru	13.68	8.625	<u>314</u>	<u>0.364</u>	<u>0.230</u>	<u>1.300</u>
BranchGRPO-DepPru	13.68	8.625	<u>314</u>	<b>0.369</b>	<b>0.231</b>	<b>1.319</b>

Table 1: Efficiency–quality comparison under identical data, rewards, and optimization schedules. Best and second-best per column are in **bold** and underline. Speedup is relative to DanceGRPO (tf=1.0). NFE counts the expected number of denoising steps where the policy is updated; for branching methods this is an *effective* NFE that reflects split density and shared prefixes.

$1 \times 10^{-4}$ ) with bf16 precision and EMA weights stored on CPU. All GRPO-related hyperparameters are kept identical across methods, with full details deferred to the supplementary material.

### 4.3 MAIN RESULTS

Table 1 compares efficiency and alignment quality across methods, while Figure 1 shows reward dynamics during training. BranchGRPO achieves consistently better alignment than DanceGRPO while using substantially fewer function evaluations and shorter iteration times. MixGRPO improves efficiency but at the cost of weaker alignment, whereas BranchGRPO provides a more favorable balance, and pruning variants further reduce computation without hurting performance.

The reward curves in Figure 1 also highlight the stability of our approach. DanceGRPO with reduced timestep fractions suffers from strong reward fluctuations, while the full-timestep variant converges more smoothly but at much higher cost. BranchGRPO combines the best of both, offering faster reward growth and more stable trajectories. Figure 4 further illustrates qualitative improvements: compared with Flux and DanceGRPO, our method produces more faithful, detailed, and coherent generations across diverse prompts.

Taken together, these results demonstrate that BranchGRPO is both more efficient and more stable than existing GRPO variants, yielding superior preference alignment under significantly reduced computational overhead.

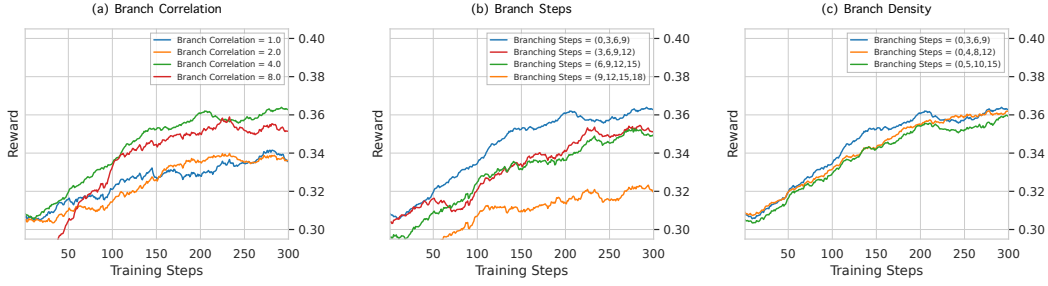


Figure 5: Ablation on branching hyperparameters *without pruning*. (a) Moderate correlation ( $s=4$ ) best balances exploration and stability. (b) Early split schedules yield higher rewards than late splits. (c) Denser early branching accelerates reward growth while converging to similar final levels.

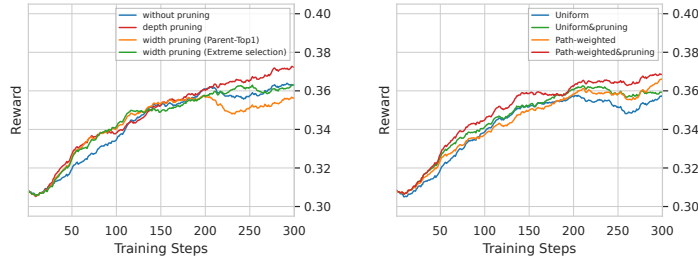


Figure 6: Ablations on pruning and reward fusion. **Left:** pruning policies (none, depth, width-Parent-Top1, width-Extreme- $b$ ). **Right:** reward-fusion strategies (uniform vs. path-weighted, with/without width pruning). Depth pruning achieves the best final reward, while path-weighted fusion improves stability across settings.

#### 4.4 ABLATION STUDIES

We conduct a series of ablation studies to better understand the design choices in BranchGRPO. Unless otherwise stated, all experiments are carried out under the same training setup as in Section 4.3. The following analyses highlight how different branching configurations and aggregation strategies affect efficiency, reward quality, and stability.

**Branch Correlation.** Figure 5(a) shows the effect of varying the branch correlation  $s$ . Smaller values ( $s = 1.0, 2.0$ ) limit exploration and lead to slower reward growth, while very large values ( $s = 8.0$ ) destabilize early training. A moderate setting ( $s = 4.0$ ) achieves the best trade-off, reaching the highest reward and stable convergence, confirming that stochastic branching is necessary but should be carefully tuned.

**Branching Steps.** We next vary the positions of split timesteps (Figure 5(b)). Early splits such as  $(0, 3, 6, 9)$  promote faster reward increase in the early stage, whereas later splits like  $(9, 12, 15, 18)$  delay exploration and yield lower rewards. Intermediate schedules (e.g.,  $(3, 6, 9, 12)$ ) balance efficiency and reward quality, suggesting that early splits are generally more effective for exploration.

**Branch Density.** Finally, we compare different densities of split points while keeping the overall horizon fixed (Figure 5(c)). Although all configurations eventually converge to similar reward levels, denser splits (e.g.,  $(0, 3, 6, 9)$ ) accelerate early training, while sparser configurations converge more slowly. This indicates that increasing the density of branching in the early phase improves sample efficiency without harming stability.

**Path-weighted vs. Uniform Fusion.** Figure 6 (right) compares uniform averaging with path-probability weighting under identical training settings. Uniform averaging shows higher variance and a clear late-stage plateau, whereas path-weighted fusion delivers consistently higher and



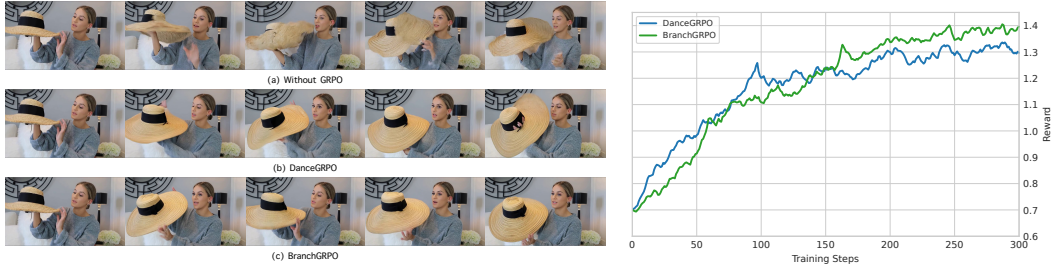


Figure 7: Video generation results on WanX-1.3B I2V. Left: qualitative frame comparisons across three settings. (a) Without GRPO: severe temporal flickering and deformation. (b) DanceGRPO: improved but still inconsistent and blurry details. (c) BranchGRPO: sharper and temporally coherent frames. Right: reward curves showing faster convergence and higher final rewards with BranchGRPO compared to DanceGRPO.

more stable rewards throughout training. This empirically supports Sec. 3.3: uniform averaging is exploration-friendly but noisy, while path weighting aligns credit assignment with the behavior distribution and improves convergence at no extra cost.

**Pruning.** Figure 6 (left) evaluates pruning applied *after* depth-wise normalization and only for backprop. *Depth pruning* (sliding window over denoising steps) achieves the **best final reward**, consistently surpassing the no-pruning baseline by reallocating compute to informative early steps while preserving forward sampling diversity. *Width pruning (Parent-Top1)* halves gradient updates and yields the smoothest, lowest-variance curve, but its final reward is slightly below depth pruning. *Width pruning (Extreme-b)* keeps the globally best and worst  $b$  leaves; it injects strong positive/negative signals and remains competitive at the end, but exhibits higher variance than the other settings.

#### 4.5 VIDEO GENERATION RESULTS

We further evaluate BranchGRPO on video generation using WanX-1.3B I2V (Wan et al., 2025). We compare three settings: the base model, DanceGRPO, and BranchGRPO. Figure 7 presents qualitative frames and quantitative reward curves.

Qualitatively, the base model exhibits severe temporal flickering, while DanceGRPO partially improves consistency but still struggles with detail preservation. BranchGRPO produces sharper frames with coherent objects across time.

Quantitatively, BranchGRPO achieves faster convergence and higher rewards, measured by the Video-Align motion quality metric (Liu et al., 2025b), confirming the benefit of branching rollouts for video generation.

### 5 CONCLUSION

We introduced **BranchGRPO**, a reinforcement learning framework that mitigates reward sparsity and rollout inefficiency in diffusion and flow models. By reformulating rollouts as tree-structured trajectories with reward fusion and lightweight pruning, BranchGRPO achieves denser credit assignment, faster convergence, and higher alignment quality at lower cost. These results establish BranchGRPO as a stable, efficient alternative to existing GRPO variants and a step toward scalable preference optimization for complex generative tasks.

---

## REFERENCES

- Kevin Black, Michael Janner, Yilun Du, Ilya Kostrikov, and Sergey Levine. Training diffusion models with reinforcement learning. *arXiv preprint arXiv:2305.13301*, 2023.
- Paul F Christiano, Jan Leike, Tom Brown, Miljan Martic, Shane Legg, and Dario Amodei. Deep reinforcement learning from human preferences. *Advances in neural information processing systems*, 30, 2017.
- Ying Fan, Olivia Watkins, Yuqing Du, Hao Liu, Moonkyung Ryu, Craig Boutilier, Pieter Abbeel, Mohammad Ghavamzadeh, Kangwook Lee, and Kimin Lee. Dpok: Reinforcement learning for fine-tuning text-to-image diffusion models. *Advances in Neural Information Processing Systems*, 36:79858–79885, 2023.
- Arthur Gretton, Karsten M Borgwardt, Malte J Rasch, Bernhard Schölkopf, and Alexander Smola. A kernel two-sample test. *The journal of machine learning research*, 13(1):723–773, 2012.
- Jonathan Ho, Ajay Jain, and Pieter Abbeel. Denoising diffusion probabilistic models. *Advances in neural information processing systems*, 33:6840–6851, 2020.
- Yuval Kirstain, Adam Polyak, Uriel Singer, Shahbuland Matiana, Joe Penna, and Omer Levy. Pick-a-pic: An open dataset of user preferences for text-to-image generation. 2023.
- Junzhe Li, Yutao Cui, Tao Huang, Yinping Ma, Chun Fan, Miles Yang, and Zhao Zhong. Mixgrpo: Unlocking flow-based grpo efficiency with mixed ode-sde. *arXiv preprint arXiv:2507.21802*, 2025a.
- Yizhi Li, Qingshui Gu, Zhoufutu Wen, Ziniu Li, Tianshun Xing, Shuyue Guo, Tianyu Zheng, Xin Zhou, Xingwei Qu, Wangchunshu Zhou, et al. Treepo: Bridging the gap of policy optimization and efficacy and inference efficiency with heuristic tree-based modeling. *arXiv preprint arXiv:2508.17445*, 2025b.
- Yaron Lipman, Ricky TQ Chen, Heli Ben-Hamu, Maximilian Nickel, and Matt Le. Flow matching for generative modeling. *arXiv preprint arXiv:2210.02747*, 2022.
- Jie Liu, Gongye Liu, Jiajun Liang, Yangguang Li, Jiaheng Liu, Xintao Wang, Pengfei Wan, Di Zhang, and Wanli Ouyang. Flow-grpo: Training flow matching models via online rl. *arXiv preprint arXiv:2505.05470*, 2025a.
- Jie Liu, Gongye Liu, Jiajun Liang, Ziyang Yuan, Xiaokun Liu, Mingwu Zheng, Xiele Wu, Qiulin Wang, Wenyu Qin, Menghan Xia, et al. Improving video generation with human feedback. *arXiv preprint arXiv:2501.13918*, 2025b.
- Runtao Liu, Haoyu Wu, Ziqiang Zheng, Chen Wei, Yingqing He, Renjie Pi, and Qifeng Chen. Videodpo: Omni-preference alignment for video diffusion generation. In *Proceedings of the Computer Vision and Pattern Recognition Conference*, pp. 8009–8019, 2025c.
- Xingchao Liu, Chengyue Gong, and Qiang Liu. Flow straight and fast: Learning to generate and transfer data with rectified flow. *arXiv preprint arXiv:2209.03003*, 2022.
- Long Ouyang, Jeffrey Wu, Xu Jiang, Diogo Almeida, Carroll Wainwright, Pamela Mishkin, Chong Zhang, Sandhini Agarwal, Katarina Slama, Alex Ray, et al. Training language models to follow instructions with human feedback. *Advances in neural information processing systems*, 35: 27730–27744, 2022.
- Rafael Rafailov, Archit Sharma, Eric Mitchell, Christopher D Manning, Stefano Ermon, and Chelsea Finn. Direct preference optimization: Your language model is secretly a reward model. *Advances in neural information processing systems*, 36:53728–53741, 2023.
- Robin Rombach, Andreas Blattmann, Dominik Lorenz, Patrick Esser, and Björn Ommer. High-resolution image synthesis with latent diffusion models. In *Proceedings of the IEEE/CVF conference on computer vision and pattern recognition*, pp. 10684–10695, 2022.

- 
- Zhihong Shao, Peiyi Wang, Qihao Zhu, Runxin Xu, Junxiao Song, Xiao Bi, Haowei Zhang, Mingchuan Zhang, YK Li, Yang Wu, et al. Deepseekmath: Pushing the limits of mathematical reasoning in open language models. *arXiv preprint arXiv:2402.03300*, 2024.
- Bram Wallace, Meihua Dang, Rafael Rafailov, Linqi Zhou, Aaron Lou, Senthil Purushwalkam, Stefano Ermon, Caiming Xiong, Shafiq Joty, and Nikhil Naik. Diffusion model alignment using direct preference optimization. In *Proceedings of the IEEE/CVF Conference on Computer Vision and Pattern Recognition*, pp. 8228–8238, 2024.
- Team Wan, Ang Wang, Baole Ai, Bin Wen, Chaojie Mao, Chen-Wei Xie, Di Chen, Fei Wu Yu, Haiming Zhao, Jianxiao Yang, Jianyuan Zeng, Jiayu Wang, Jingfeng Zhang, Jingren Zhou, Jinkai Wang, Jixuan Chen, Kai Zhu, Kang Zhao, Keyu Yan, Lianghua Huang, Mengyang Feng, Ningyi Zhang, Pandeng Li, Pingyu Wu, Ruihang Chu, Ruili Feng, Shiwei Zhang, Siyang Sun, Tao Fang, Tianxing Wang, Tianyi Gui, Tingyu Weng, Tong Shen, Wei Lin, Wei Wang, Wei Wang, Wenmeng Zhou, Wenten Wang, Wenting Shen, Wenyuan Yu, Xianzhong Shi, Xiaoming Huang, Xin Xu, Yan Kou, Yangyu Lv, Yifei Li, Yijing Liu, Yiming Wang, Yingya Zhang, Yitong Huang, Yong Li, You Wu, Yu Liu, Yulin Pan, Yun Zheng, Yuntao Hong, Yupeng Shi, Yutong Feng, Zeyinzi Jiang, Zhen Han, Zhi-Fan Wu, and Ziyu Liu. Wan: Open and advanced large-scale video generative models. *arXiv preprint arXiv:2503.20314*, 2025.
- Xiaoshi Wu, Yiming Hao, Keqiang Sun, Yixiong Chen, Feng Zhu, Rui Zhao, and Hongsheng Li. Human preference score v2: A solid benchmark for evaluating human preferences of text-to-image synthesis, 2023.
- Jiazheng Xu, Xiao Liu, Yuchen Wu, Yuxuan Tong, Qinkai Li, Ming Ding, Jie Tang, and Yuxiao Dong. Imagereward: learning and evaluating human preferences for text-to-image generation. In *Proceedings of the 37th International Conference on Neural Information Processing Systems*, pp. 15903–15935, 2023.
- Zeyue Xue, Jie Wu, Yu Gao, Fangyuan Kong, Lingting Zhu, Mengzhao Chen, Zhiheng Liu, Wei Liu, Qiushan Guo, Weilin Huang, et al. Dancegrpo: Unleashing grpo on visual generation. *arXiv preprint arXiv:2505.07818*, 2025.

## A APPENDIX

This appendix provides additional theoretical proofs, implementation details, and experimental results that complement the main paper. The contents are organized as follows:

- **Section B:** Hyperparameter settings used in all experiments.
- **Section C:** Theoretical analysis, including proofs for branch noise construction, reward fusion, and variance reduction.
- **Section D:** Additional experiments, including ablations, more text-to-image and image-to-video results.
- **Failure Cases:** Qualitative examples where BranchGRPO fails, highlighting current limitations.

## B HYPERPARAMETER SETTINGS

Table 2 summarizes the detailed hyperparameter configuration used in our experiments. All hyperparameters are kept identical across all methods, including **DanceGRPO** and **MixGRPO**, to ensure a fair comparison.

Table 2: Hyperparameter settings used in all experiments.

Parameter	Value	Parameter	Value
Random seed	42	Learning rate	$1 \times 10^{-5}$
Train batch size	2	Weight decay	$1 \times 10^{-4}$
SP size	1	Mixed precision	bfloat16
SP batch size	2	Grad. checkpointing	Enabled
Dataloader workers	4	Max grad norm	0.01
Grad. accum. steps	12	Warmup steps	0
Checkpoint steps	40	Use TF32	Yes
Resolution	$720 \times 720$	Sampling steps	16
Eta	0.3	Sampler seed	1223627
Num. generations	12	Shift (branch offset)	3
Use group reward	Yes	Ignore last step	Yes
Clip range	$1 \times 10^{-4}$	Adv. clip max	5.0
Use EMA	Yes	EMA decay	0.995
Init same noise	Yes		

## C THEORETICAL ANALYSIS (DETAILED PROOFS)

### C.1 BRANCH NOISE CONSTRUCTION AND BOUNDARY DISTRIBUTION PRESERVATION

Consider the reverse SDE discretized by Euler–Maruyama:

$$z_{i+1} = \mu_\theta(z_i, t_i) + g_i \eta_i, \quad \eta_i \sim \mathcal{N}(0, I), \quad g_i := g(t_i) \sqrt{h_i}. \quad (6)$$

At a split step  $i \in B$ , we construct  $K$  branch noises as

$$\xi_b = \frac{\xi_0 + s \delta \xi_b}{\sqrt{1 + s^2}}, \quad \xi_0, \delta \xi_b \stackrel{i.i.d.}{\sim} \mathcal{N}(0, I), \quad (7)$$

so that  $\xi_b \sim \mathcal{N}(0, I)$  for each  $b$ , and  $\text{Cov}(\xi_b, \xi_{b'}) = \frac{1}{1+s^2} I$  for  $b \neq b'$ .

Each child branch then updates as

$$z_{i+1}^{(b)} = \mu_\theta(z_i, t_i) + g_i \xi_b. \quad (8)$$

---

**Lemma 1** (Single-step marginal preservation). *For any fixed parent  $z_i$ , we have*

$$z_{i+1}^{(b)} \stackrel{d}{=} \mu_\theta(z_i, t_i) + g_i \eta_i, \quad \eta_i \sim \mathcal{N}(0, I).$$

**Lemma 2** (Leaf marginal preservation). *Conditioned on prefix  $(z_0, \eta_0, \dots, \eta_{i-1})$ , each branch  $z_N^{(b)}$  generated by the split rule has the same distribution as a baseline SDE sample  $z_N$ .*

**Theorem 1** (Boundary distribution invariance). *Under the branching construction above, for any set of split steps  $B$ , each leaf  $z_N^{(b)}$  has the same marginal law as a baseline SDE rollout. Hence, branching does not alter the final generator distribution.*

## C.2 REWARD FUSION: UNBIASEDNESS AND VARIANCE REDUCTION

Let  $L(n)$  be the leaf set of a node  $n$ . Each leaf has reward  $r_\ell = r(z_N^{(\ell)})$ . Define the conditional expected return

$$V(n) := \mathbb{E}[r(z_N) \mid n].$$

**Uniform fusion.**

$$\bar{r}(n) = \frac{1}{|L(n)|} \sum_{\ell \in L(n)} r_\ell. \tag{9}$$

Then

$$\mathbb{E}[\bar{r}(n) \mid n] = V(n), \quad \text{Var}(\bar{r}(n) \mid n) = \frac{\sigma^2(n)}{|L(n)|},$$

where  $\sigma^2(n) = \text{Var}(r_\ell \mid n)$ .

**Path-probability weighted fusion.** If leaves are drawn from proposal  $q(\ell \mid n)$  with weights

$$w_\ell = \frac{p_{\text{beh}}(\ell \mid n)}{q(\ell \mid n)},$$

then the IS estimator

$$\hat{r}_{\text{IS}}(n) = \frac{1}{|L(n)|} \sum_{\ell \in L(n)} w_\ell r_\ell$$

is unbiased:  $\mathbb{E}[\hat{r}_{\text{IS}}(n) \mid n] = V(n)$ . The self-normalized IS estimator

$$\hat{r}_{\text{SNIS}}(n) = \frac{\sum_\ell w_\ell r_\ell}{\sum_\ell w_\ell}$$

is consistent with variance  $O(1/\text{ESS})$ , where

$$\text{ESS} = \frac{(\sum_\ell w_\ell)^2}{\sum_\ell w_\ell^2}.$$

## C.3 DEPTH-WISE BASELINE (CONTROL VARIATES)

For  $K$  siblings at depth  $i$ , let fused returns  $\bar{r}^{(b)}$ , and group mean  $\bar{r}_i = \frac{1}{K} \sum_b \bar{r}^{(b)}$ . Define

$$A_i^{(b)} = \bar{r}^{(b)} - \bar{r}_i, \quad \sum_b A_i^{(b)} = 0. \tag{10}$$

Let  $g_i^{(b)}(\theta) = \nabla_\theta \log p_\theta(\text{branch } b \text{ at depth } i)$ . Then

$$\widehat{\nabla J}_{\text{group}} = \frac{1}{K} \sum_{b=1}^K A_i^{(b)} g_i^{(b)}$$

is an unbiased gradient estimator with strictly smaller variance than  $\widehat{\nabla J}_{\text{single}} = \frac{1}{K} \sum_b \bar{r}^{(b)} g_i^{(b)}$ , unless  $\text{Cov}(\bar{r}^{(b)}, g_i^{(b)}) = 0$ .

#### C.4 CONTINUOUS REWARDS AND CONCENTRATION

Assume  $r$  is  $L$ -Lipschitz and the SDE flow  $\Psi_{i+1 \rightarrow N}$  is  $K_i$ -Lipschitz. Then

$$|r(z_N^{(b)}) - r(z_N^{(b')})| \leq LK_i g_i \|\xi_b - \xi_{b'}\|.$$

Thus  $r(z_N^{(b)})$  is sub-Gaussian with parameter  $\mathcal{O}(L^2 K_i^2 g_i^2)$ . Averaging over  $|L(n)|$  leaves gives

$$\Pr(|\bar{r}(n) - V(n)| \geq \varepsilon \mid n) \leq 2 \exp(-c \cdot |L(n)| \varepsilon^2 / (L^2 K_i^2 g_i^2)).$$

## D ADDITIONAL EXPERIMENTS

### D.1 MORE QUANTITATIVE RESULT

Table 3 reports more results.

Table 3: Ablation study of BranchGRPO under different design choices. Best and second-best per column are in **bold** and underline. All results are obtained under the same training setup as in Section 4.3.

Configuration	NFE $_{\pi_{\theta_{\text{old}}}}$	NFE $_{\pi_{\theta}}$	Iteration Time (s) $\downarrow$	HPS-v2.1 $\uparrow$	Pick Score $\uparrow$	Image Reward $\uparrow$	CLIP Score $\uparrow$
<i>Branch Density</i>							
(0, 3, 6, 9)	13.68	13.68	493	<u>0.363</u>	0.229	<u>1.233</u>	<u>0.374</u>
(0, 4, 8, 12)	11.56	11.56	416	0.359	0.229	1.238	0.374
(0, 5, 10, 15)	9.44	9.44	340	0.354	0.228	1.220	0.366
<i>Reward Fusion</i>							
Uniform Fusion	13.68	13.68	493	0.361	0.229	1.218	0.368
Path-Weighted Fusion	13.68	13.68	493	<u>0.363</u>	0.229	<u>1.233</u>	<u>0.374</u>
<i>Pruning Strategy</i>							
Width Pruning	13.68	8.625	<u>314</u>	<u>0.364</u>	<u>0.230</u>	<u>1.300</u>	<u>0.374</u>
Depth Pruning	13.68	8.625	<b>314</b>	<b>0.369</b>	<b>0.231</b>	<b>1.319</b>	<b>0.381</b>



## D.2 MORE TEXT2IMAGE RESULTS

An anime man in flight uniform with hyper detailed digital artwork and an art style inspired by Klimt, Nixeu, Ian Spriggen, Wlop, and Krenz Cushart.



Flux

DanceGRPO

BranchGRPO(Ours)

A raccoon riding an oversized fox through a forest in a furry art anime still.



Flux

DanceGRPO

BranchGRPO(Ours)

Totem pole made out of cats.



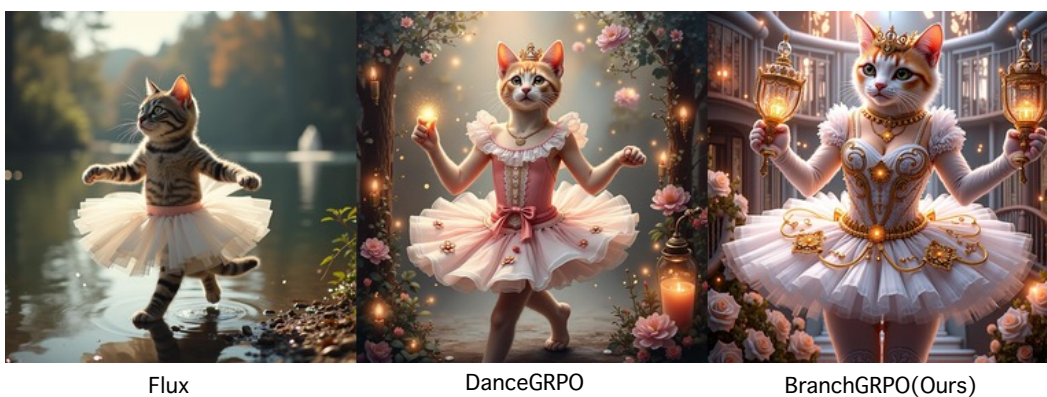
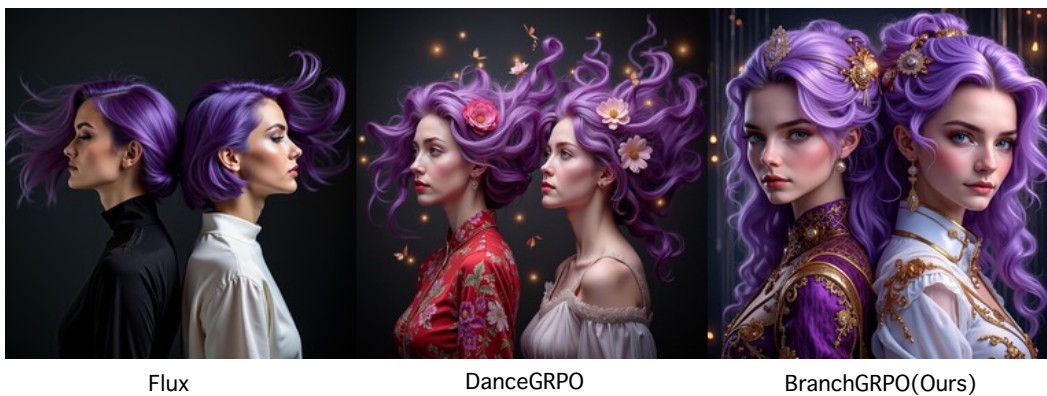
Flux

DanceGRPO

BranchGRPO(Ours)

Figure 8

A portrait of two women with purple hair flying in different directions against a dark background.



A cute anime schoolgirl with a sad face submerged in dark pink and blue water, portrayed in an oil painting style.

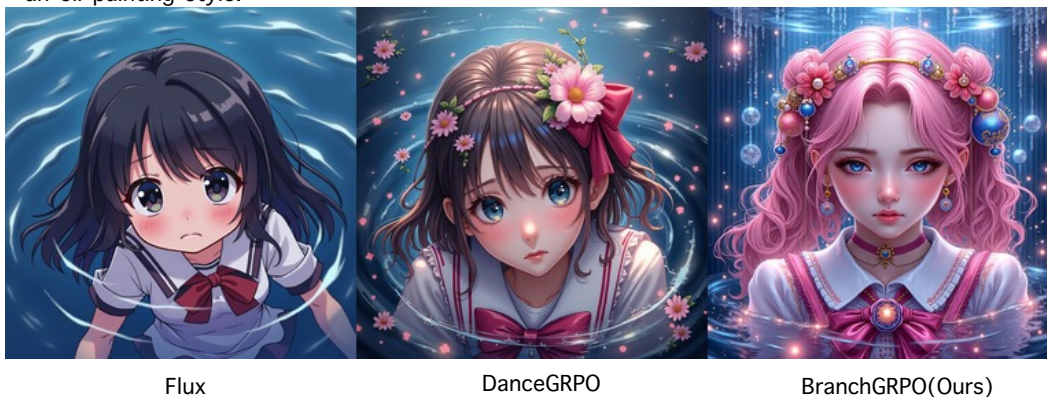


Figure 9



The image is of a raccoon wearing a Peaky Blinders hat, surrounded by swirling mist and rendered with fine detail.

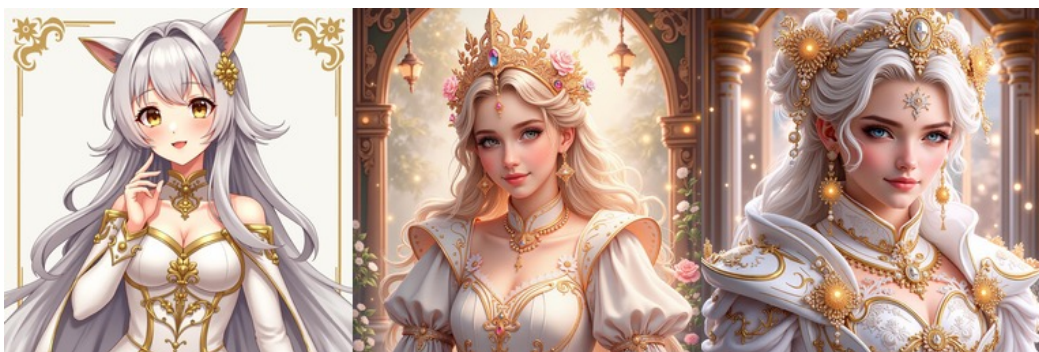


Flux

DanceGRPO

BranchGRPO(Ours)

Portrait of an anime princess in white and golden clothes.



Flux

DanceGRPO

BranchGRPO(Ours)

A cute little anthropomorphic Tropical fish knight wearing a cape and a crown in short, pale blue armor.



Flux

DanceGRPO

BranchGRPO(Ours)

Figure 10

A white polar bear cub wearing sunglasses sits in a meadow with flowers.



Flux

DanceGRPO

BranchGRPO(Ours)

A photo of a mechanical angel woman with crystal wings, in the sci-fi style of Stefan Kostic, created by Stanley Lau and Artgerm.

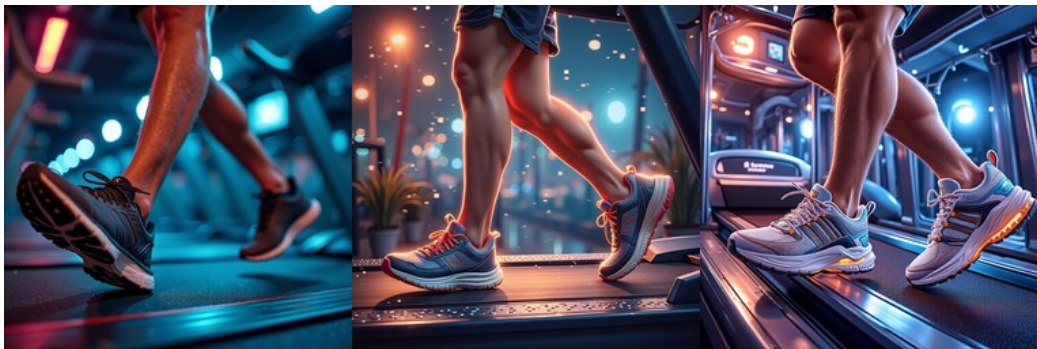


Flux

DanceGRPO

BranchGRPO(Ours)

Close-up shot of a person running on a treadmill with worn running shoes under dramatic lighting and a comic book-style painting effect.



Flux

DanceGRPO

BranchGRPO(Ours)

Figure 11



Family assembling missile in living room.



Flux

DanceGRPO

BranchGRPO(Ours)

The image depicts alien flowers and plants surrounded by visceral exoskeletal formations in front of mythical mountains with dramatic contrast lighting, created with surreal hyper detailing in a 3D render.



Flux

DanceGRPO

BranchGRPO(Ours)

A colorful tin toy robot runs a steam engine on a path near a beautiful flower meadow in the Swiss Alps with a mountain panorama in the background, captured in a long shot with motion blur and depth of field.



Flux

DanceGRPO

BranchGRPO(Ours)

Figure 12

---

### D.3 MORE IMAGE2VIDEO RESULTS



(a) Case 1



(b) Case 2



(c) Case 3





Without GRPO



BranchGRPO

(a) Case 4



Without GRPO

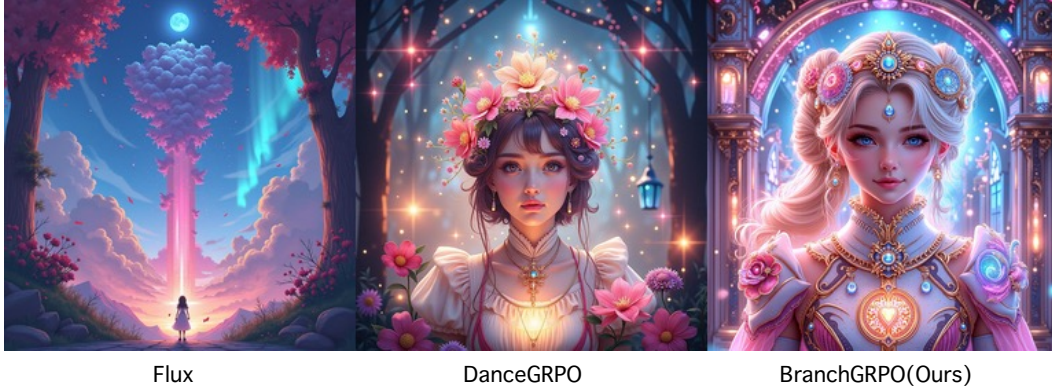


BranchGRPO

(b) Case 5

#### D.4 FAILURE CASES

A colorful digital painting with a front view and anime-inspired vibes featuring a magical composition.



A one-eyed dwarf wizard holding a flagon in clean cel shaded vector art.



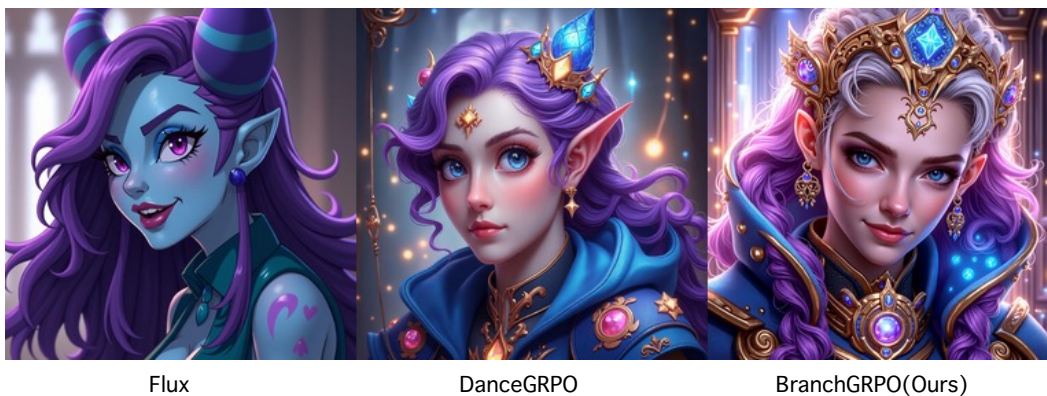
Australian soldiers surrendering to an emu.



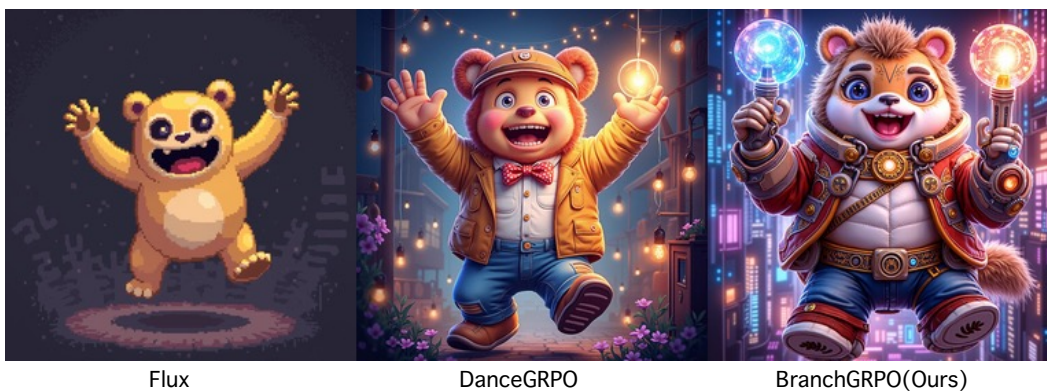
Figure 15: Failure case



Head and shoulders portrait of Jinx from League of Legends of Arcane animated Series.



The image is of Pixel Art Huggy Wuggy performing a jumpscare.



A 3D render of a volcanic icon on a rocky background, in isometric perspective and darkly lit.

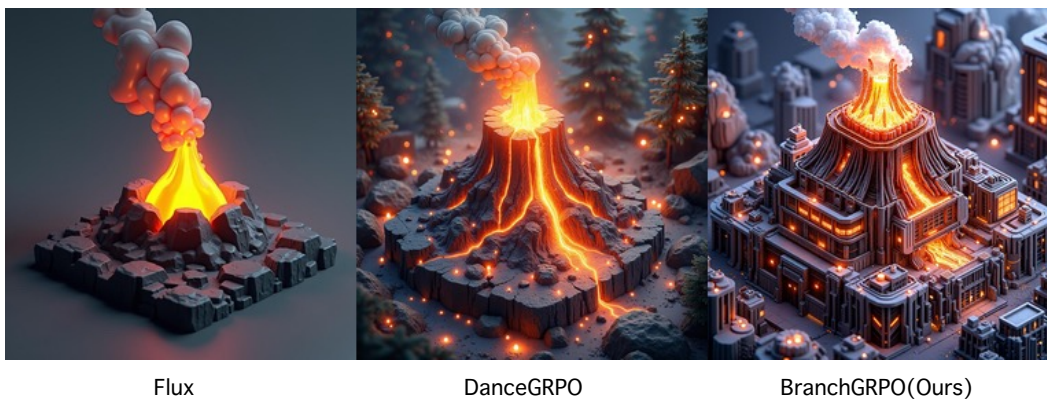


Figure 16: Failure case